Developing a Hail and Wind Damage Swath Event Database from Daily MODIS True Color Imagery and Storm Reports for Impact Analysis and Applications

JORDAN R. BELL,[a] EMILY F. WISINSKI,[b] ANDREW L. MOLTHAN,[a] CHRISTOPHER J. SCHULTZ,[a] EMMA GILLIGAN,[c] AND KAYLEE G. SHARP[d]

[a] *Earth Science Branch, NASA Marshall Space Flight Center, Huntsville, Alabama*
[b] *Department of Atmospheric and Earth Science, University of Alabama in Huntsville, Huntsville, Alabama*
[c] *Department of Geography and Environmental Systems, University of Maryland, Baltimore County, Baltimore, Maryland*
[d] *Earth System Science Center, University of Alabama in Huntsville, Huntsville, Alabama*

(Manuscript received 1 December 2022, in final form 2 June 2023, accepted 14 June 2023)

ABSTRACT: Hail and damaging winds are two threats associated with intense and severe thunderstorms that traverse the Midwest and Great Plains during the primary growing season. In certain severe thunderstorm events, large swaths of agricultural crops are impacted, allowing the damage to be viewed from multiple satellite remote sensing platforms. Previous studies have focused on analyzing individual hail and wind damage swaths (HWDSs) using satellite remote sensing, but these swaths have never been officially archived or documented. This lack of documentation has made it difficult to analyze the spatial extent and temporal frequency of HWDSs from year to year. This study utilizes daily true color imagery from MODIS aboard NASA's *Terra* and *Aqua* satellites and daily local storm reports from the Storm Prediction Center to build a database of HWDSs occurring in the months of May–August, for years 2000–20. This database identified 1646 HWDSs in 12 states throughout the Midwest and Great Plains, confirmed through a combination of archived severe weather warnings, radar information, and official storm reports. For each entry in the HWDS database, a geospatial outline is provided along with the most likely date of first visible damage from MODIS imagery as well as the physical characteristics and time of occurrence estimated from available warnings. This study also provides a summary of the radar characteristics for a portion of the database. This database will further the understanding of severe weather damage by hail and wind to agriculture to help understand the frequency of these events and assist in mapping the impacted areas.

SIGNIFICANCE STATEMENT: Hail and wind damage swaths (HWDSs) frequently occur during the primary growing season throughout the Midwest and Great Plains but are not yet officially documented or tracked like other severe weather impacts (e.g., tornadoes and derechos). This study describes the creation of a 21-yr HWDS event database using archived daily storm reports and daily true color satellite imagery. Once the database was completed and underwent quality checks, the research team identified spatial and temporal trends from the confirmed swaths.

KEYWORDS: Climatology; Hail; Geographic information systems (GIS); Remote sensing; Agriculture; Thunderstorms

1. Introduction

Intense and severe thunderstorms routinely produce extensive monetary losses throughout the United States. In 2016, these losses were estimated at $11.23 billion (U.S. dollars), comparable to losses associated with hurricanes in the same year (Gunturi and Tippett 2017). Hail and wind damage is a significant contributor to losses from thunderstorms, estimated to exceed $10 billion annually when including all of North America (Loomis 2018). Many of these economic impacts result from damage to property and agriculture. In 2022, agricultural crop losses attributed to hail, hurricanes, and severe weather exceeded $1 billion (American Farm Bureau Federation 2023). This is concerning as an estimated 20 000 severe thunderstorms occur in the United States annually, and many occur during the primary growing season (May–August) for the Great Plains and the Midwest (Kelly et al. 1985). The frequency, intensity, seasonality, and resulting impacts from severe weather have motivated numerous studies to quantify their occurrence and trends.

Studies within the United States during the 1960s and 1970s quantified hail occurrence nationwide, with regional focus in the Midwest and Great Plains. Frisby (1962) examined a decade of insurance records in South Dakota, separating ground damage patterns to agricultural crops into various groups. Each group was associated with a corresponding synoptic-scale pattern (e.g., fast moving cold front, slow moving frontal system, or near the apex of low pressure systems), though these patterns often occurred without producing hail, damaging winds, or a damage swath. In cases where a swath occurred, Frisby (1963) documented ranges from 80 to 321 km (50–200 mi) in length and 8–24 km (5–15 mi) in width. Changnon and Stout (1967) analyzed insurance statistics provided by the Crop-Hail Insurance Actuarial Association for 7 years for 14 wheat- and 9 corn-producing states. During the May–October growing season, hail intensity and the crop's growth stage increased the susceptibility to damage during the months of July for corn (June–July for wheat) states. Previous research also examined how hail damage

Denotes content that is immediately available upon publication as open access.

Corresponding author: Jordan R. Bell, jordan.r.bell@nasa.gov

DOI: 10.1175/WAF-D-22-0210.1

to vegetation was impacted by accompanying winds. Changnon (1967) used a hail observation network to show that strong surface winds in conjunction with hail fall had more impact on crop damage than hail size and hail fall duration. Towery et al. (1976) showed that agricultural crop losses were 3–12 times greater when impacted by wind-driven hail than the areas of the crops that were shielded by larger objects.

Changnon (1971) analyzed damage swaths in the 1960s from aerial photography using both standard color and infrared film. Another study leveraging aerial-based photography was conducted in the mid- to late 1970s, focused on performing quantitative damage assessments to assist the insurance sector. This study overlapped with the introduction of computers being used to assist with mapping and generating crop damage statistics (Towery 1980). Computer procedures were able to combine and derive damage estimates from aerial photography, improving the impact analysis on swaths of severe weather impacted agricultural crops. Procedures and methodology used in these studies are similar to ones used today for analyzing the impacts as satellite remote sensing capabilities are now routinely available from geostationary (GEO) and low-Earth orbit (LEO) satellites.

The availability of global land surface remote sensing at increasingly higher spatial resolution has led to a growing volume of case studies examining hail and wind damage swaths. Klimowski et al. (1998) used the 1-km visible channel from the *GOES-8* satellite to observe a damage swath that was measured over 120 km in length and 7–11-km width that occurred in South Dakota in 1996. Subsequent analyses have utilized the red-visible and near-infrared bands common across many land surface observing missions, with sensitivity to vegetation health and chlorophyll as measured by the normalized difference vegetation index (NDVI; Rouse et al. 1974; Tucker 1979). NDVI ranges from -1 in pixels of clouds or water, to near zero for little to no green vegetation, up to a value of 1 for pixels comprised primarily of healthy, dense, and green vegetation.

Bentley et al. (2002) used pre- and post-storm *Landsat-7* ETM+ 30-m imagery to derive NDVI change where decreases in NDVI corresponded with NOAA *Storm Data* wind and hail reports. They focused on mapping damage swaths for the meteorological and insurance communities. Parker et al. (2005) used a rolling 7-day maximum NDVI 250-m composite from MODIS to map two damage swaths from the July 2003 severe weather events in South Dakota. With the use of additional modeling, potential meso- to storm-scale impacts were hypothesized. Gallo et al. (2012) compared 7-day MODIS NDVI losses of 0.021–0.357 over Iowa in August 2009 and related them in space and time to local NOAA *Storm Data* reports and radar-estimated hail size. Molthan et al. (2013) differenced postevent NDVI from a previous 20-day NDVI composite, and related loss of NDVI to the maximum estimated size of hail (MESH) radar product (Witt et al. 1998). Decreased NDVI occurred alongside increases in radar-estimated hail size. Bell and Molthan (2016) produced damage maps using a kernel filter applied to single-day MODIS NDVI and land surface temperature, with greatest success in densely vegetated agricultural zones late in the growing season. Gallo et al. (2019) used a detailed series of ground photography to relate categories of observed hail and wind damage NDVI decreases ranging from 0.12 to 0.28. Bell et al. (2020) further examined new signals of NDVI change compared to synthetic aperture radar backscatter from ESA's Sentinel-1 satellite mission, noting that changes occur due to structural damage to crops from combined hail and wind damage, but that the direction of change may be further impacted by soil moisture and antecedent precipitation or irrigation.

The aforementioned studies have documented the long-standing history and evolving approaches of using satellite remote sensing to identify the occurrence of hail and wind damage to agriculture, providing the opportunity to fill gaps in storm reporting (Ortega et al. 2009). In the United States, where there is a dense network of ground-based weather radars, and derived radar products such as MESH, MRMS (Smith et al. 2016), and Multi-Year Reanalysis of Remotely Sensed Storms (MYRORSS; Williams et al. 2022) can provide approximate locations of potential hail fall for individual case studies. MRMS and MYRORSS can also be used to derive climatologies at a higher spatial resolution and provide additional information about the temporal and spatial occurrence of hail (Murillo and Homeyer 2019; Tang et al. 2019; Murillo et al. 2021). LEO passive microwave satellite missions such as TRMM (Cecil and Blankenship 2012) and the GPM mission (Bang and Cecil 2019) core observatory and constellation of international partners has been used to create a nearly worldwide map of hail frequency through brightness temperature observations.

To expand upon these methods and explore the spatial and temporal frequency of these events, this study develops a methodology for identifying damage swaths visible from NASA's *Terra* and *Aqua* MODIS, confirmed through best effort combination of NOAA/Storm Prediction Center Storm Reports, NOAA's NEXRAD radar products, and NOAA's National Weather Service (NWS) severe thunderstorm and tornado warnings. Through manual identification of visible hail and wind damage swaths from MODIS, and the likelihood of occurrence confirmed by other NOAA data, the result is a regional database of damage swaths for the Midwest and Great Plains. The combined swath information is used to address the following research questions:

- How many damage swaths are visible from MODIS across these regions? How do the damage swaths vary annually and, on a month-to-month basis during the growing season?
- How do these damage swath occurrences vary in general shape, length, width, and area?
- What are some characteristics of the storms, as inferred by radar, as to when the damage most likely occurred for each event?

This study characterizes regional variability and frequency of damage swaths and offers a new dataset that can aid in the identification and understanding of the environmental conditions that produce intense and severe thunderstorms leading to these impactful damage swaths over agricultural areas. Observations from MODIS support future efforts to automate hail and wind damage detection from similar (e.g., VIIRS, GOES ABI) and other higher-resolution sensors (e.g.,

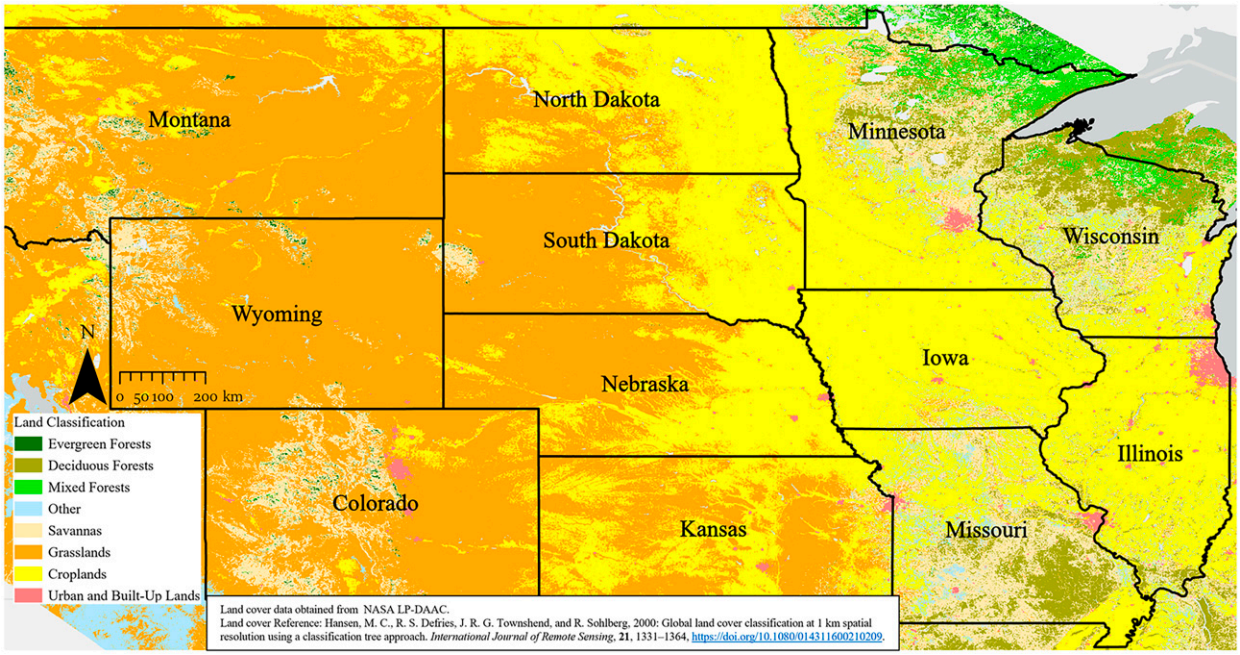

FIG. 1. Map of the 12 states in this study with corresponding landcover (Hansen et al. 2000).

Landsat, Sentinel-2, Planet) available from a growing constellation of public and private sector investments.

2. Data and methods

a. Study area

This study focused on an area of interest (AOI) that spans the Midwest and Great Plains (Fig. 1), from the Rocky Mountains to the Great Lakes and from Kansas through the Dakotas. The AOI is made up of a bounding box between 85°–113°W longitude and 35.8°–50°N latitude. It includes the entirety of 11 states (Wyoming, Colorado, North Dakota, South Dakota, Nebraska, Kansas, Minnesota, Iowa, Missouri, Wisconsin, and Illinois) and a portion of one state (Montana) analyzed during a 21-yr time period. The selection of this AOI aligns with a study of spatial and temporal trends of severe weather reports from 1989 to 2018, which found the peak probability of large hail (damaging winds) in this region occurs May–August (mid-June–August; Taszarek et al. 2020).

Consistent with the emphasis on agriculture in this study, cropland and grasslands are the two primary landcover classifications across the AOI. Another prominent land class includes forests, especially in Minnesota, Wisconsin, and Missouri (Fig. 1). The uniformity and consistency of the land cover provides the opportunity to evaluate the land surface for potential damage swaths. The risk for severe weather impacts is highest during the primary growing season when seasonal agriculture has developed a uniform, green canopy. In the selected AOI, this often results in damage producing a stark visual contrast against a more uniform background. Damage swaths have been observed visually in satellite imagery in other regions (e.g., southern plains, Southeast) primarily in the early spring, when surface vegetation conditions make it very difficult to discern impacts and changes resulting from severe weather.

b. NASA MODIS imagery

Combined from the *Terra* and *Aqua* missions, MODIS provides global opportunities to observe Earth's surface up to four times per day, with red and near-infrared bands at the highest spatial resolution (nadir; 250 m), complemented by additional true color bands (blue and green) at 500 m, and a broader range of near- to thermal-infrared bands at 1 km. Our efforts to catalog potential events focused on visible interpretation of imagery, therefore, we leveraged NASA's Worldview tool, an interactive data portal from NASA's Earth Observing System Data and Information System (EOSDIS), which provides over 1000 products from polar and geostationary satellites. Special emphasis is given to low-latency products such as those from MODIS, allowing for rapid generation of recent observations while also offering an archive of imagery back through the observing record.

Specifically, we used NASA's Worldview derived MODIS true color (bands 4, 3, 1) and false color (bands 7, 2, 1) composites. Worldview imagery from *Terra*/MODIS dates back to 24 February 2000 while imagery from *Aqua*/MODIS became available on 3 July 2002. *Terra* had periods of outages, which prevented MODIS daily observations from occurring, in August 2000 and June 2001 (MODAPS Services 2022). Worldview also offers data visualization services such as a slider to compare between two dates of imagery; for our work, this capability allowed for comparing pre- and postevent scenes to visually confirm sudden change potentially caused by severe weather. When a suspected damage scar was identified, Worldview tools were used to identify the date that the scar was first visible in any *Terra* or *Aqua* MODIS scene (FirstDate, Table 1),

TABLE 1. Description of three different dates that were acquired for each event in the hail and wind damage swath database.

Metadata field	Description
SwathDate	Date that the hail damage swath most likely occurred. This date will match the SPC event date (1200–1159 UTC) with the corresponding storm reports (if available)
FirstDate	The swath first appears in MODIS true color imagery
BestDate	Subjectively, the best appearance in MODIS true color imagery up to 15 days after the SwathDate, and potentially the same as FirstDate

and an additional date when we felt that the appearance of the damage swath was best visualized (BestDate, Table 1). These efforts were necessary because a particularly large scar could be partially obscured by cloud cover or off-nadir views on any given day, which resulted in a lower resolution depiction. Imagery from the BestDate was extracted in GeoTIFF format from Worldview and then used to assist in the manual creation of geospatial outlines of the visible damage swath as it appeared in the imagery. Each geospatial outline is an entry in the database.

c. SPC storm reports

Analysis of damage swaths through Worldview resulted in a FirstDate and BestDate, but questions still remained about when the severe thunderstorm actually occurred. This was particularly challenging when a swath appeared after multiple days of cloud cover. Additional information was used to estimate a SwathDate, defined as the most likely date that the damage was produced by severe weather, based upon assessment of additional evidence.

Local storm reports (LSRs) were a logical starting point. NOAA/NWS/Storm Prediction Center (SPC) LSRs were examined to hypothesize the approximate date and time of the associated severe weather event. While LSRs were a useful first step, there are regions where population densities are very low, and severe weather reports are limited (Cintineo et al. 2012). Further, public estimates of hail size may be underrepresented both spatially and temporally when compared to observations from ground radars (Witt et al. 1998). LSRs were reviewed using traditional online reports and graphics (https://www.spc.noaa.gov/climo/reports/) with reports in the last 10 years viewed through their interactive online viewer (https://www.spc.noaa.gov/exper/reports/). For the years of 2012–17, we also examined an SPC experimental product comparing hail LSRs to MESH values greater than 2.54 cm (1 in.; https://www.spc.noaa.gov/climo/online/lsrmesh/).

d. Storm events database

The National Centers for Environmental Information (NCEI) maintains the Storm Events Database. This database, first released in 1999, aggregates historical records and documents the occurrence of storms, severe weather, and other significant weather phenomena, that may have caused injuries, loss of life, or significant property damage. The database is populated using local and preliminary storm reports from the SPC and local Weather Forecast Offices. These reports are then quality controlled before being finalized. This database makes up NOAA's monthly publication, *Storm Data*.

e. NCEI/NEXRAD storm features

While SPC local storm reports and other SPC report products (interactive viewer and LSR-MESH relationships) were helpful in estimating the SwathDate, additional radar information was sought to confirm the likely occurrence of hail. To determine the proximity of hail to suspected hail and wind damage swaths, additional data were acquired from the NCEI Severe Weather Data Inventory—specifically, through the use of their REST web services and queries of the NEXRAD Level-3 hail signatures (nx3hail). Level-3 maximum size point data were acquired for the suspected SwathDate and a bounding box comprising the damage scar area. Signatures were plotted for each damage swath event and visually confirmed in proximity to the scar apparent in MODIS. The direction of the storm and hail scar implied by the NEXRAD products were comparable to that observed in the MODIS imagery. The hail signatures product also includes information such as hail probability and size, but for this study, only the geographic extent, orientation, and timing were used to visually confirm that the SwathDate was appropriate for the hail scar observed by MODIS.

f. NOAA/National Weather Service severe thunderstorm and tornado warnings

The Iowa Environmental Mesonet (IEM) at Iowa State University (https://mesonet.agron.iastate.edu/) provides an extensive series of data archives and web-based services that include a multitude of archived NWS text products, past severe weather warnings, and other meteorological data. While not an official archive of NOAA/NWS information, IEM's records are among the most extensive, openly available, and easy to use for acquiring a historical record of NOAA/NWS watch and warning information. IEM's online displays of archived warnings and radar information were used to help confirm the correct event date (SwathDate) for a suspected hail scar. In addition, we used IEM to acquire shapefiles for county-scale and storm-based severe thunderstorm or tornado warnings dating back to 2000. These shapefiles were used to create our own overlaying displays. These displays combined MODIS imagery, NCEI/NEXRAD storm features, and *Storm Data* reports to confirm that hail or wind-driven damage was the most likely culprit in the production of the observed damage swaths. Many of the previous studies (Bentley et al. 2002; Parker et al. 2005; Gallo et al. 2012; Molthan et al. 2013; Bell and Molthan 2016; Gallo et al. 2019; Bell et al. 2020) denoted that hail and damaging winds were both contributors to damage swaths; therefore, going forward in this manuscript, they will be known as hail and wind damage swaths (HWDSs).

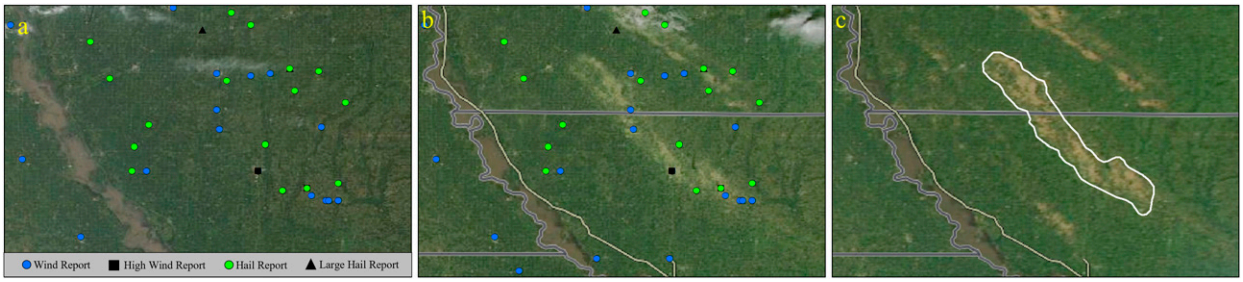

FIG. 2. (a) Storm Prediction Center Storm Reports and MODIS true color imagery for 18 Aug 2011 (SwathDate) in northwestern Missouri, southeastern Nebraska, and southwestern Iowa. (b) Visible HWDSs on 19 Aug 2011 by MODIS true color imagery (FirstDate). (c) Same HWDSs as in (b), but observed on 24 Aug 2011 by MODIS true color imagery (BestDate) with the geospatial outline drawn around one of the HWDSs.

For damage swaths that included one or more overlapping severe weather warnings, we used the time of first overlapping warning issuance to assume the time the damage began. Warnings provided greater and more consistent geospatial overlap than other point-sources of hail information such as those from NEXRAD Level-3 products or *Storm Data* reports.

g. *MRMS data*

Daily MRMS data were acquired from 2001 to 2010 from the free and open MYRORRS dataset recently available from NOAA and their partnership with Amazon/AWS (s3://noaa-oar-myrorss-pds; Ortega et al. 2023). For the first half of the HWDS database, the SwathDate was used to select the date and corresponding 24-h period of MRMS products from 1200 UTC to 1159 UTC the following day, corresponding to the coverage of daily storm reports. Fields acquired focused on characteristics of hail-producing thunderstorms including the MESH product, vertically integrated liquid (VIL), and the reflectivity at the lowest altitude. For each MRMS field, products were accumulated and aggregated as the maximum value. MRMS product values were extracted at grid points contained within each HWDS. Here, we constrained our analysis of radar characteristics to the top 25% (169) largest HWDS events (2001–10) by area; that is, the largest swaths that occurred in the first 10 years of the database. As archival access to MRMS products grows over time, additional MRMS fields and temporal coverage can be added to expand the availability of radar-inferred characteristics for each HWDS event.

h. *Combining data to create and confirm HWDS events*

A four-step approach was used to identify and document possible HWDSs in the *Terra/Aqua* MODIS record from 1 May to 31 August of each year, 2000–20. This time frame was selected to encompass the primary growing season for the region. Clusters of SPC LSRs, especially those arranged in a linear fashion similar to the visual appearance of a damage swath, were selected as areas of interest (Fig. 2a). MODIS imagery, using NASA's Worldview tool, was examined for up to 15 days after the date of the LSRs, with additional days added in cases of extensive cloud cover. This period includes time for the vegetation to decay (turn brown) and minimizes extensive recovery time, similar to previous efforts in detecting vegetation damage (Bell and Molthan 2016). Apparent HWDSs in MODIS true color imagery were catalogued and further scrutinized using the Worldview comparison tool for two different dates of MODIS imagery. Additional information for each swath included whether *Terra* or *Aqua* observed the potential swath and any relevant local SPC Storm Reports. Three specific dates were cataloged for each potential swath: 1) when the swath occurred (SwathDate, Fig. 2a), 2) the swath was visible for the first time in the MODIS satellite imagery (FirstDate; Fig. 2b), and 3) the date the swath exhibits the best appearance in MODIS imagery (BestDate; Fig. 2c). Potential HWDSs were subjectively reviewed and evaluated by three collaborators, who each assigned a subjective confidence rating using a range of integers from 0 to 10. After the evaluation of the 21-yr period, potential swaths with low to moderate confidence values (<6) were reassessed and some were selected for removal. Some reasons for removal included discovery that the potential swath was a misidentification of a permanent land feature or because there was insufficient other data (e.g., validating severe weather warnings, radar data, or *Storm Data* reports) to support confirmation.

BestDate MODIS imagery from Worldview were downloaded and imported into Esri's ArcGIS Pro (https://www.esri.com/en-us/arcgis/products/arcgis-pro/overview), a geographic information system (GIS) software used to create shapefile polygons to outline the potential HWDSs. For long swaths of damage, but with small gaps visible along the path, multiple polygons were drawn to outline the damage. Metadata attributes were included for each polygon to align information with the damaged area (Table 1).

This process resulted in over 1800 potential HWDSs. As a second quality control process, each HWDS polygon and MODIS image selected from the BestDate was used to create a product combining satellite imagery with NOAA/NWS severe weather warnings (via IEM), NEXRAD Level-3 hail maximum size, and *Storm Data* reports for the proposed SwathDate. If the potential damage polygon had at least one overlapping severe thunderstorm or tornado warning, NEXRAD Level-3 hail indicators, or a report from *Storm Data* within the vicinity, the HWDS was confirmed and retained in the final database. If the proposed SwathDate did not result in these indicators aligning with the damage polygon, the SwathDate was reassessed. Warning information was checked for the week before and after the proposed SwathDate (±7 days), and overlapping warnings in this extended

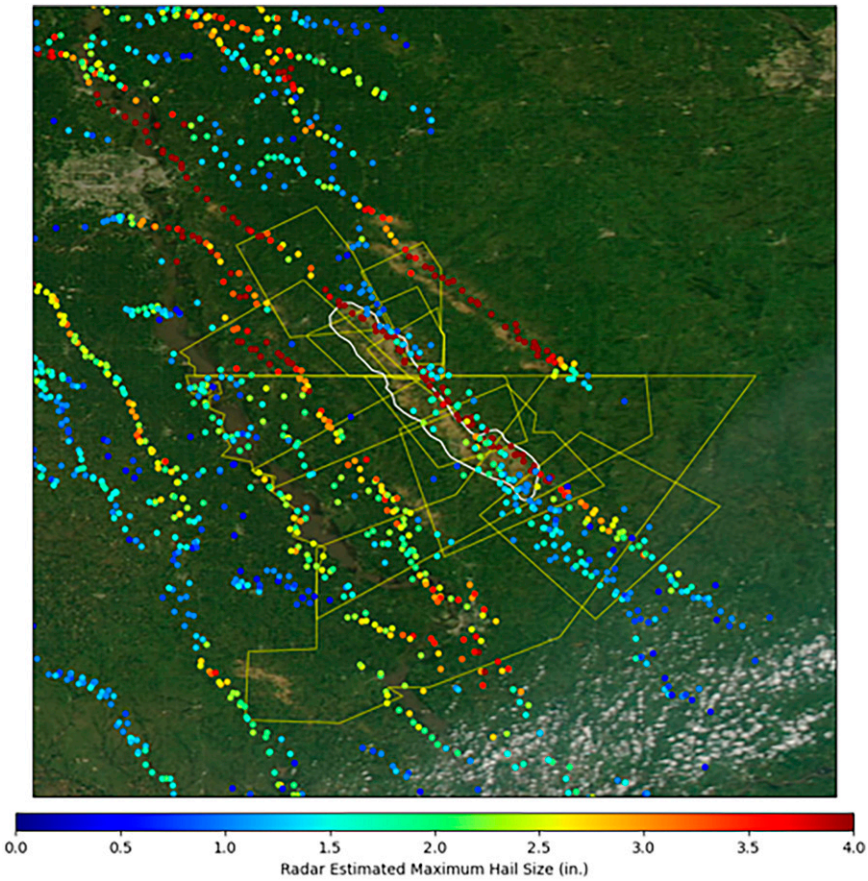

FIG. 3. Same geospatial outline as Fig. 2, but with archived severe thunderstorm warnings and NEXRAD Level-3 radar estimated maximum hail size (in.) features overlayed to confirm the date and location of the HWDS.

period served as new potential SwathDate information (Fig. 3). A total of 21 (1.3%) HWDSs did not have severe thunderstorm or tornado warnings available from the IEM sources but were confirmed using the other datasets. Archived radar and warning information were reexamined to select the date that appeared as the most likely source for the event. Through an iterative process, SwathDate was reevaluated to choose the most likely event date from overlaps of the damage polygon, MODIS imagery, NWS warnings, LSRs, and NEXRAD Level-3 features.

3. Analysis of database

A total of 1646 confirmed HWDSs were identified and included in the events database (Fig. 4). This analysis section will focus on the physical characteristics such as length, width, and area of each identified HWDS, time of occurrence, and spatial extent.

a. Length, width, and area

Frisby (1962) first denoted "swath-type patterns with a northwest to southeast slant," "slightly curved lines or series of lying southwest to northeast," and "clusters without easily recognizable form." All confirmed HWDSs in the database were labeled into four different categories based on the perceived shape of the swath (Figs. 4 and 5): 1) circular, 2) complex, 3) curved, and 4) linear.

Red and yellow lines compare two different methodologies for estimating swath lengths and widths. Yellow lines depict team member analyst efforts to manually measure features using ArcGIS Pro (Fig. 5). For nearly circular or elliptical swaths (Fig. 5a), the two longest axes were measured and the shortest of the two was designated as the width and the longer assigned as the length. Complex swaths (Fig. 5b) often had multiple appendages and odd shapes. Analysts did their best to measure the longest axis of the polygon for the length and the widest portion of the polygon perpendicular to the length as the width. Curved and linear polygons (Figs. 5c,d) used the centerline measurement from the polygon and acquired the width as the perpendicular measurement made at the widest point. Curved swaths were those that had one or more clear bends between the start and end of the swath but could be measured along a single, continuous centerline.

Manual methods were compared to automated approaches using Python geospatial libraries (geopandas and shapely). For each swath, libraries were used to construct a minimum bounding rectangle (MBR) with the length (longest side) and width (shortest side) retained as metrics (Fig. 5; red outlines).

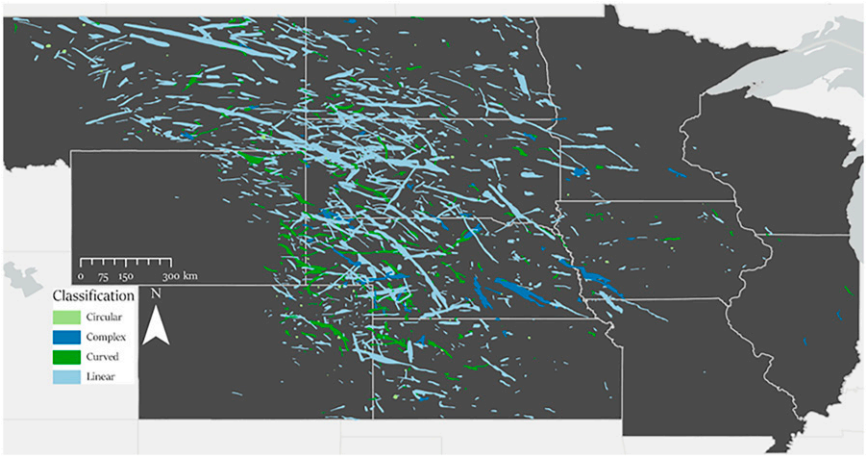

FIG. 4. Map of confirmed HWDSs in the event database classified by shape of the swath.

This methodology was the most efficient in terms of effort and computation in obtaining lengths and widths for all the swaths in the database.

Length measurements from the two methodologies were strongly correlated (r^2 = 0.98–0.99; Figs. 6a–d). MBRs generate a similar length regardless of the complexity of the shape. Width measurements had larger discrepancies (Figs. 6e–h). The circular classification width measurements, with an r^2 of 0.94, had less variation than the linear and complex classifications measurements, with their respective r^2 values being 0.85 and 0.82 and the curved classification with an r^2 of 0.41. Many of the curved HWDS classifications had varying widths between the two methods because the MBR's shortest axis would be larger based on the amount of curvature, while in the manual method, the widest part of the outline could be identified and measured (Fig. 5c). Automated methods for determining length and width can introduce various errors (i.e., measurement estimation). This could be mitigated with further evaluation of the additional machine vision tools.

A summary of the two methods used for determining length and width and a summary of swath area is available in the appendix. The average swath length measured was 29.0 (28.7) km manually (MBR) with a range of 2.1–372.5 (2.1–377.3) km. The average swath width measured was 6.1 (6.8) km manually (MBR) with a range of 1.4–29.5 (1.5–37.0) km. Given the complexities in swath shapes and difficulties in addressing them through MBRs, this study opts to use the manual measurements via ArcGIS Pro to be consistent with the manual approach used to map and measure tornado damage pathlengths and widths. Figure 7 shows the distribution of HWDS lengths and widths using both methodologies for each measurement broken down by shape classification. The overall trend in both methodologies was that the greater the length of the HWDS the greater the width. The only differences between the two methodologies were in the number of counts that made up each bin.

The area of each swath was calculated using ArcGIS Pro. The average area of each swath in the database was 160.6 km^2. Areas for the entire database ranged from 3.2 to 4996.3 km^2. A total of 1036 (63.0%) swaths had an area under 100 km^2 with 728 (44.2%) swaths having an area between 25 and 100 km^2 (Fig. 8). Only 34 (2.1%) of the database had an area extent exceeding 1000 km^2.

b. *Spatial extent of HWDSs*

Confirmed HWDSs were identified in all 12 states within the AOI (Fig. 4). South Dakota had the most confirmed HWDSs with a count of 358, followed by 299 in Nebraska and 293 in North Dakota (Fig. 9). Swaths that crossed multiple state borders were counted toward the total in each of the states that swath touched. This is similar to how tornadoes are counted when crossing state lines and county warning areas. Missouri, Illinois, and Wisconsin ranked lowest with 9, 6, and 5 events, respectively.

Storm Data has a total of 94 521 hail reports in the study area during the same 21-yr period as the HWDS database (Fig. 10). The heaviest concentration of HWDSs overlap with the heaviest concentration of hail reports (outside of the major urban areas) across western Nebraska and South Dakota. In eastern Montana and northwestern North Dakota, hail reports become more sparse, as did the number of swaths that were cataloged. Three of the bottom four states in terms of total number of swaths (Minnesota, Missouri, and Wisconsin) were the same three states that had the largest variety of land classifications throughout (Fig. 1). The variety in land classifications across the surface may have made it difficult to detect potential HWDSs. Forested regions would not have shown a HWDS unless all of the vegetation was stripped, and the overall structure of the impacted forest was significantly altered. The density of reports and confirmed HWDSs also decreases in the eastern half of the study area, especially for northern Minnesota, Wisconsin, Illinois, and most of central and eastern Missouri (Fig. 10). The decrease in reports and limited HWDSs could be representative of reduced population in these areas being available to make reports and/or the storm environment in these areas being unable to support the intense and severe thunderstorms that produce HWDSs and/or the land cover present is less conducive to a damage swath being visible.

Gridding severe weather reports help account for biases that are related to "spatial inhomogeneities of the population

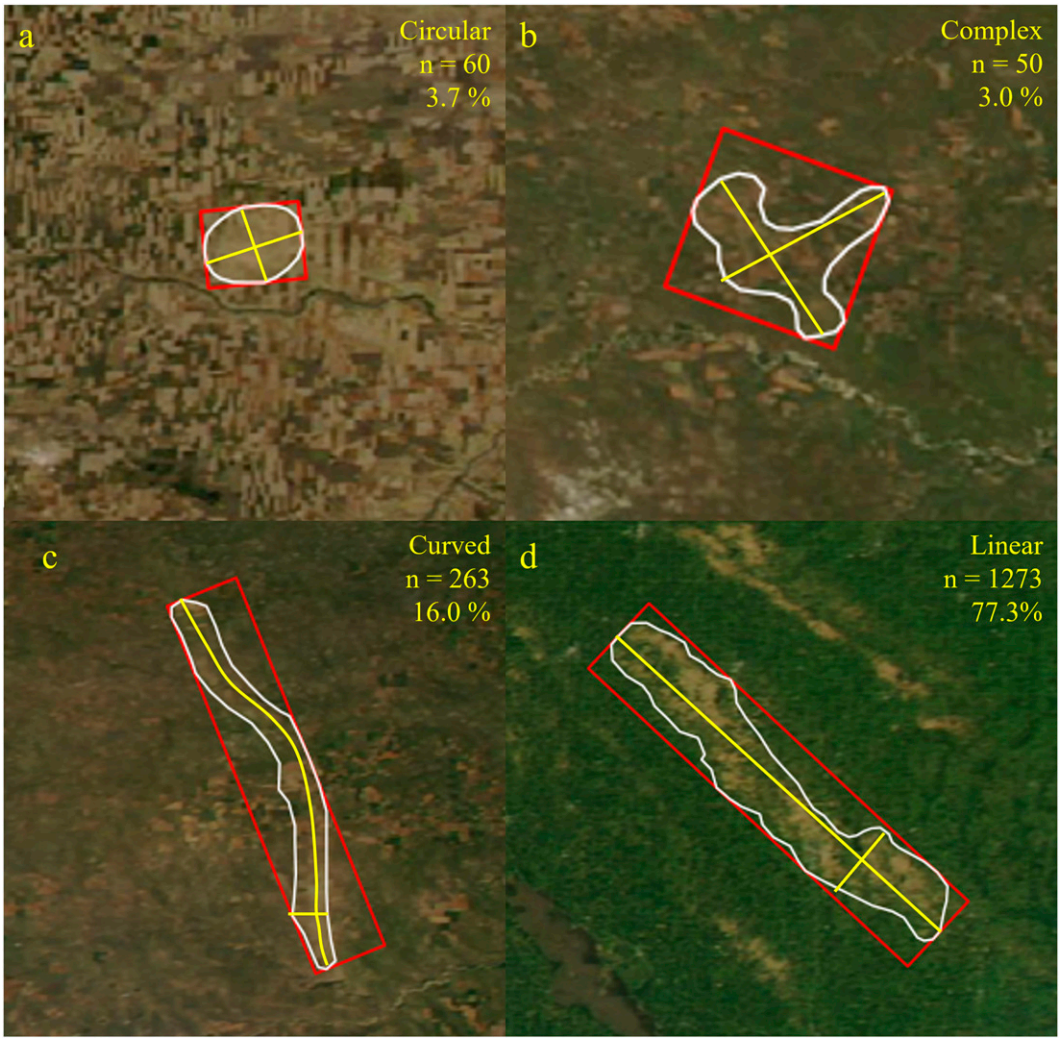

FIG. 5. (a) Example of a circular HWDS. The white outline is the geospatial boundary of the swath, yellow lines are the manual length and width measurements, and the red bounding box is the minimum bounding rectangle (MBR) method. The number of swaths in this classification and percentage of the database are in the top-right corner. (b) As in (a), but for a complex HWDS. (c) As in (a), but for a curved HWDS. (d) As in (a), but for a linear HWDS.

biased reports to be somewhat smoothed out for climatological evaluation" (Murillo et al. 2021).

To identify areas of overlap, or "local maximums," various resolution grids were tested over the areal extent of the database to count the number of swaths intersecting each grid cell (Fig. 11).

Figure 11a shows the HWDS database on a 0.25° grid, where two adjoining grid cells in northeastern Wyoming had 13 HWDSs intersect over the course of the 21-yr period, the largest occurrence of overlaps in the database. Overlaps also occurred in northwestern South Dakota near the North Dakota border (12 swaths), western South Dakota (10–11 swaths), and in parts of western Nebraska, southwestern North Dakota, and northwestern Kansas (8–10 swaths; Fig. 11b). Changnon (1972) identified this same region, northwestern Kansas, western Nebraska, and southwestern North Dakota, as the area with highest crop insurance losses between 1948 and 1967. Cintineo et al. (2012) also identified this area as having maximum hail occurrence as estimated by radar-based hail days. Conversely, the Black Hills region in southwest South Dakota had zero grid cells intersect HWDSs as there were no swaths identified over the 21 years of observations, despite numerous hail reports occurring (Fig. 10). The most likely reason for this void is the forest land cover type making it difficult to visually identify any HWDSs. There is a visible reduction in grid cell counts from west to east across the states, with 3–5 intersecting HWDSs which include eastern South Dakota, Nebraska, southwestern Minnesota, and southwestern Iowa.

c. *Temporal trends of HWDSs*

HWDS counts ranged from 34 to 126 with an average of 78.4 swaths annually. The year 2011 had the most confirmed

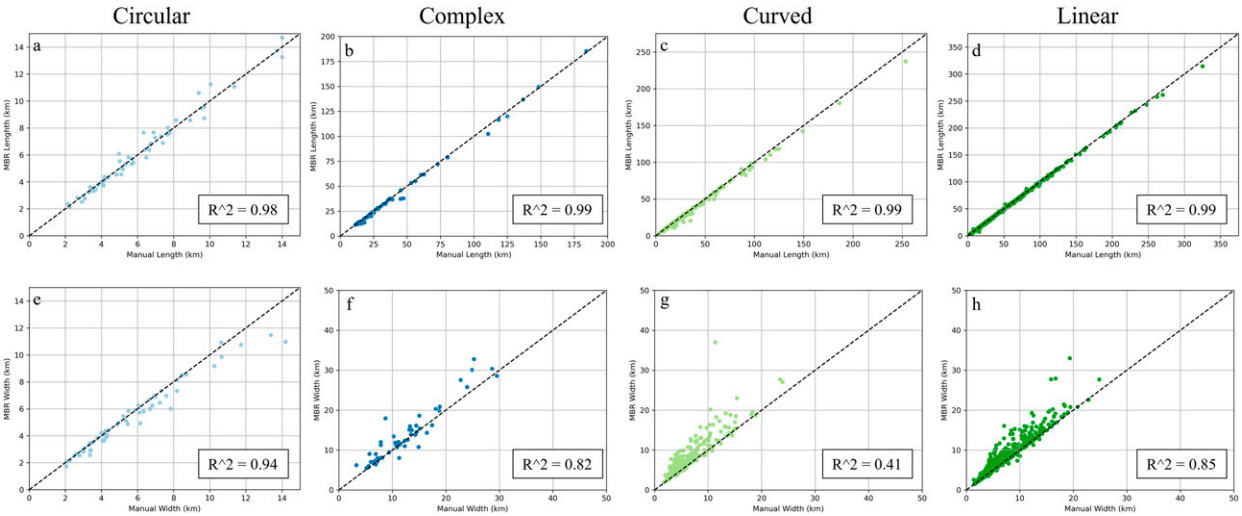

FIG. 6. (a) Scatterplot comparing circular lengths of the manual and MBR measurements. (b) As in (a), but for complex lengths. (c) As in (a), but for curved lengths. (d) As in (a), but for linear lengths. (e) Scatterplot comparing circular widths of the manual and MBR measurements. (f) As in (e), but for complex widths. (g) As in (e), but for curved widths. (h) As in (e), but for linear widths.

damage swaths followed by the years of 2010 and 2009 with 126, 124, and 121, respectively (Fig. 12). The year 2002 had the least number of identified swaths with 34, followed by 2006 and 2012 with 40 and 42, respectively. There was an overall increasing annual trend during the 21-yr time period, despite variability from year to year. The annual median was 75 swaths with a standard deviation of 28.5. Three of the 21 years had a yearly total less than one standard deviation

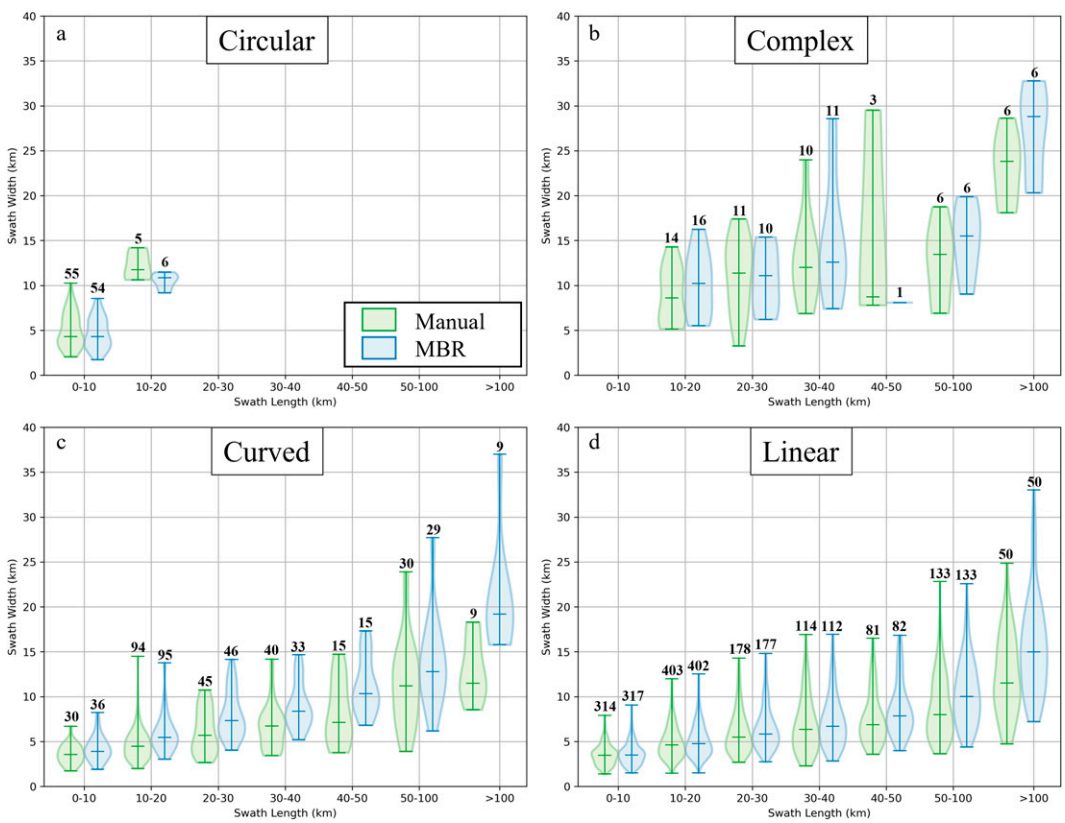

FIG. 7. (a) Distribution of circular HWDSs lengths and widths displayed as a violin plot. The number of HWDSs in each length bin are above each violin with the median value marked inside each violin. (b) As in (a), but for complex HWDSs. (c) As in (a), but for curved HWDSs. (d) As in (a), but for linear HWDSs.

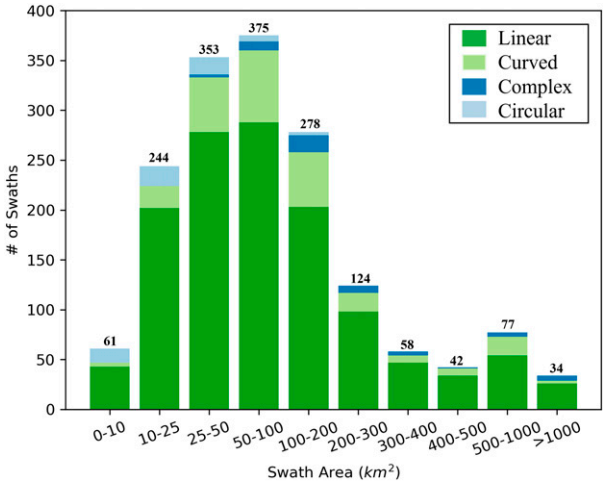

FIG. 8. Histogram of HWDSs by area and classification. The total count for each bin is on top of each bar.

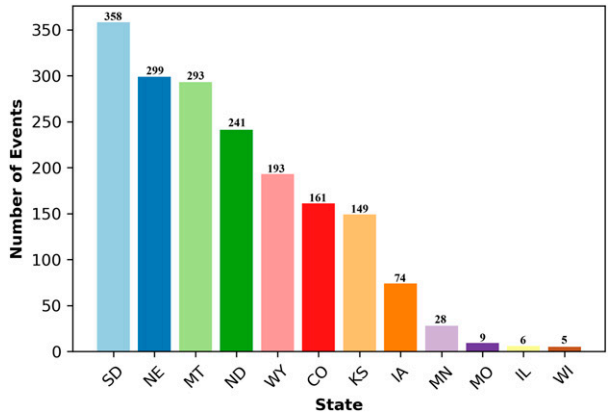

FIG. 9. Distribution of HWDS totals by state for the 21-yr time period.

below the median (46.5 swaths) and 6 years had an annual total one standard deviation above the median (103.5 swaths). In 2012 when a major drought was observed over the AOI, the number of *Storm Data* reports and HWDSs were both down compared to 2011 observations. There was no observable trend between the number of *Storm Data* hail and thunderstorm wind reports with the number of HWDSs that occurred over the AOI. (Fig. 12). Overall, for the 21 years covered in this study, there is a mix of increased and decreased *Storm Data* reports compared to the number of HWDSs.

A total of 650 HWDSs occurred during the month of July in the 21-yr period. Results in this study are consistent with Changnon (1977) who confirmed that July was the peak hail intensity considering "the … number of stones, duration of hail, wind with hail, and size of hail." and overlap in time when crops are most susceptible to damage in the states of Illinois, Minnesota, Iowa, Missouri, and Nebraska. Counts in July were followed by June (569), August (295), and May (132).

Severe weather warnings were used to estimate the time of the day that the swath occurred by using the earliest warning issuance time of intersecting warnings. This estimate identifies the warning (and ideally, the storm) most closely associated with the confirmed damage swath. Figure 13 shows there is an increase in the number of swaths that occur between 1800 and 0000 UTC with the peak of 227 confirmed swaths presumed to start between 2200 and 2300 UTC (1800–1900 CDT/1700–1800 MDT). After the peak, there is a slow decline during the late evening hours (0000–0600 UTC) and early morning (0600–1100 UTC) hours. The least number of swaths occurred just after sunrise (1100–1200 UTC; 0600–0700 CDT/0500–0600 MDT) with just one swath occurring during this time period over the course of the 21-yr study.

d. MRMS characteristics

Violin plots of MESH, VIL, and lowest altitude radar reflectivity for the largest 169 (25%) HWDSs of the 2001–10 period overlapping with MYRORRS/MESH are shown in Fig. 14. For MESH, extremes range from relatively few reports of hail 1.5 in. (12.7 mm) or smaller, including some pairs of swaths and MESH that contained no radar-estimated hail (Fig. 14a). Visual inspection of three swaths (not shown) indicates cases where there are geographic displacements between MESH estimated from radar sampling aloft, versus where hail then likely fell and impacted the surface away from the original radar location. This is similar to issues noted by Molthan et al. (2013) who observed that often the MESH-indicated hail occurred with some displacement from other public storm reports and indicators of surface damage. These occurrences were limited to regions with relatively sparse low-altitude radar coverage, such as northeastern Colorado and eastern Wyoming. Meanwhile, the interquartile range of MESH observations lying directly within an HWDS polygon spans 24.6–49.4 mm, with a median of 36.3 mm, with the majority of values exceeding the 25.4-mm (1 in.) hail size criteria for a severe thunderstorm warning. The HWDSs comprising the database primarily experience hail meeting or exceeding severe weather criteria and are therefore most often associated with severe thunderstorms. Some additional events may occur from subsevere hail sizes in combination with strong thunderstorm winds. MRMS estimates of VIL generate

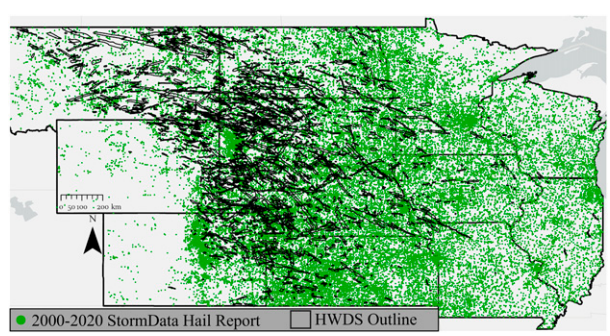

FIG. 10. Map of *Storm Data* hail reports between 2000 and 2020 with the HWDS database overlaid.

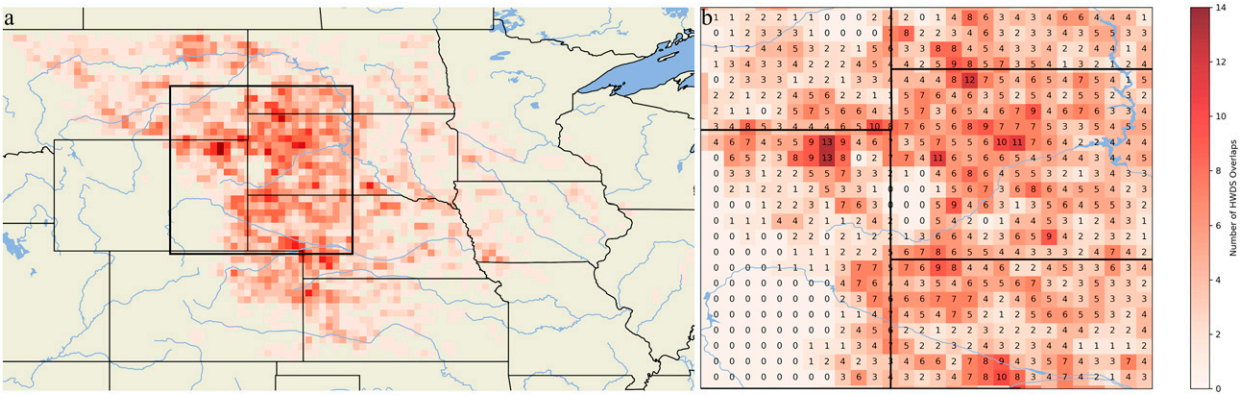

FIG. 11. (a) Gridded counts of the HWDS database. (b) Zoomed-in gridded HWDS counts over northeastern Wyoming, southeastern Montana, southwestern North Dakota, western South Dakota, and northwestern Nebraska.

an interquartile range from approximately 29.8 to 45.9 kg m^{-2}, values consistent with large volumes of ice and liquid mass within severe thunderstorms (Fig. 14b). Consistent with the MESH findings for large hail, the lowest-level radar reflectivity values are concentrated at ~58.1 dBZ (25th percentile) and higher (Fig. 14c).

3. Summary and future work

Intense and severe thunderstorms cause billions of dollars in damages from the combination of high winds and hail around the globe annually. Many of these events occur in the agricultural regions of the central United States evident as scarred vegetation viewed from satellite remote sensing true color imagery. The size, scale, location, and limited physical accessibility of these events make them ideal for assessment from satellite remote sensing platforms. Years of previous work demonstrated methods for capturing damage swath events up to several hundred kilometers long and tens of kilometers wide. These studies documented evolving approaches to using satellite remote sensing to identify the occurrence of hail and wind damage but did not capture the frequency and spatial extent annually.

To advance the understanding of these events and applicability of remote sensing, this study developed a database of HWDSs for 12 states across the Midwest and Great Plains using daily local storm reports and daily *Terra/Aqua* MODIS true color imagery. A total of 1646 hail and wind damage swaths were identified and cataloged during the warmest months of the growing seasons for the years 2000–20. Aggregation of these events over an entire year allows for predicting impacts to crop values and income during the growing season. Analysis of this database identified the following:

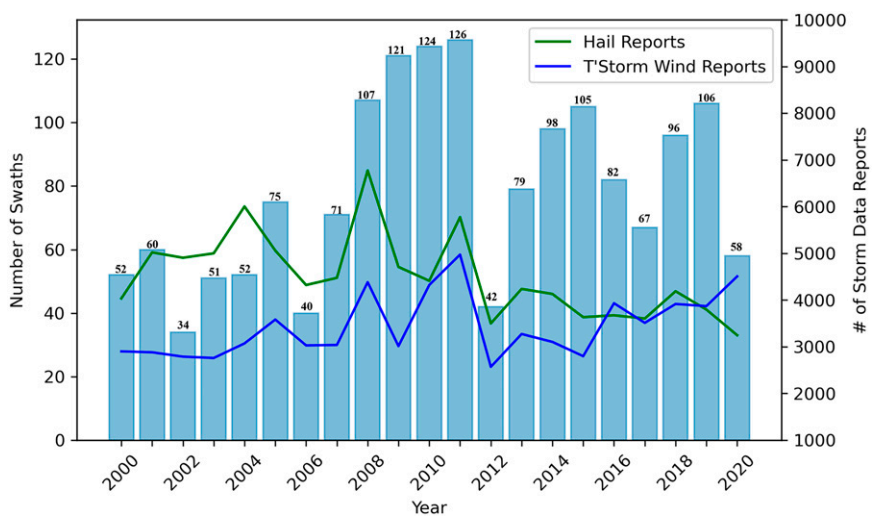

FIG. 12. Histogram of annual HWDSs between 2000 and 2020. Bold numbers represent the number of HWDSs for that year. Hail and thunderstorm wind reports from *Storm Data* are also plotted for each year.

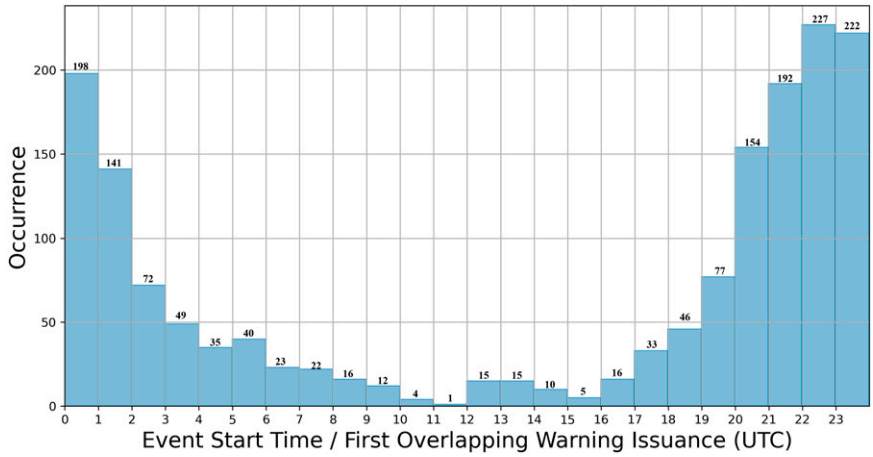

FIG. 13. Histogram of HWDSs by UTC time the swath started to occur using archived severe weather warnings.

- Length and width for each HWDS were obtained via two different methodologies (manual and MBR) and determined that both methodologies provide very similar lengths, but the manual measurement methodology provides more accurate width measurements. The mean length was 29.0 km, and the mean width of 6.1 km. The average area was computed to be 160.6 km^2.
- Maximum HWDSs occurred in northeastern Wyoming. Additional areas of high concentration of HWDSs were found in northwestern South Dakota near the North Dakota border, western South Dakota, and in parts of western Nebraska, southwestern North Dakota, and northwestern Kansas. Parts of our study where a small number or zero HWDSs were identified are the same areas that saw a reduced number confirmed hail reports during the 21-yr study.
- The number of swaths that occurred annually was highly variable with annual HWDS counts ranging from 34 to 126.

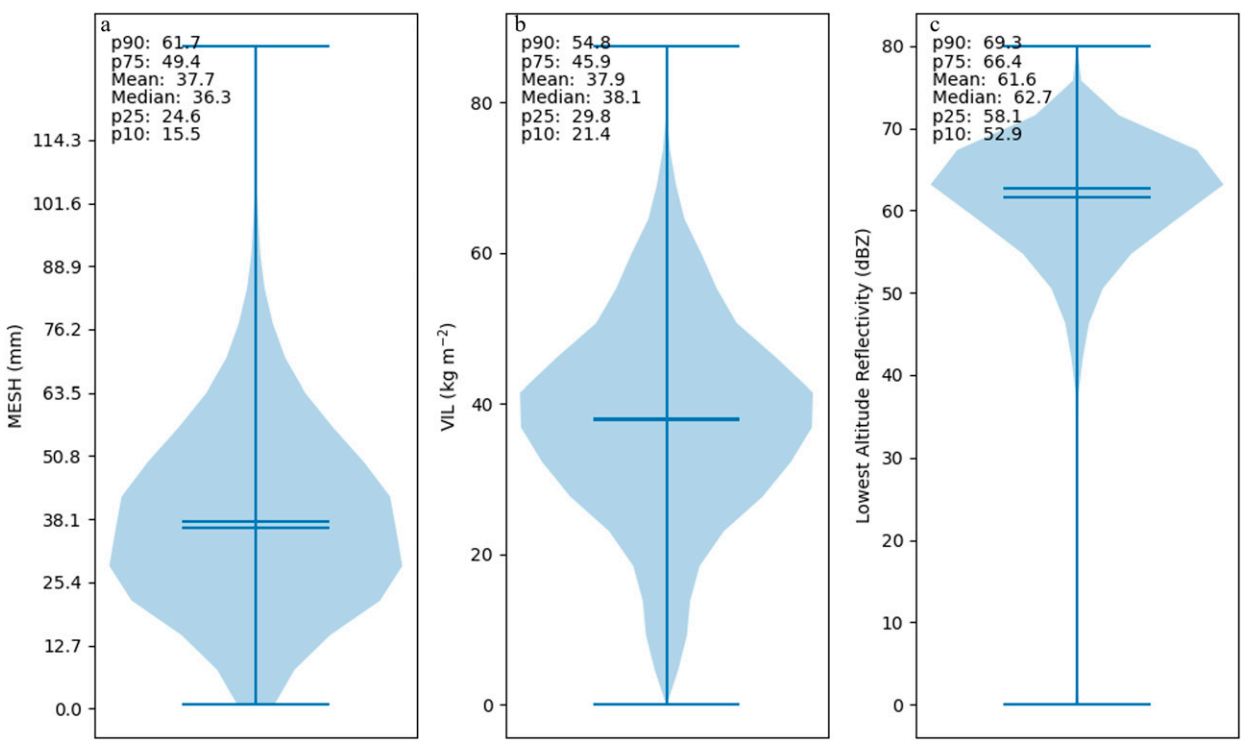

FIG. 14. (a) Violin plot showing MESH distribution for top 25% of the HWDSs by area. (b) As in (a), but for VIL. (c) As in (a), but for lowest altitude reflectivity. The horizontal lines in each violin represent the mean and median.

The occurrence of HWDSs throughout the day followed the diurnal cycle with the maximum number of HWDSs occurring between 2200 and 2259 UTC and the minimum of HWDSs occurring around 1200 UTC.

- In analyzing MRMS data for a subset of the database, most HWDSs coincide with thunderstorms that had an estimated hail size at or above the severe criteria (25.4 mm), had large volumes of ice and liquid mass (30–44 km g^{-2}) and had their lowest-level radar reflectivity values at or above 58 dB*Z*. These identified values can be useful in determining thresholds for characterizing thunderstorms that are capable of damage to agriculture.

Periodic updates from similar instruments, such as ABI and VIIRS, will help quantify events and any changes in their frequency or characteristics outside of the established HWDS database. Alignment of HWDSs with severe weather warning times sets the stage to better understand relationships of storm modes and radar characteristics, and whether unique environments or storm-scale processes exist during the creation of a HWDS. Machine learning approaches using this database as expert-labeled cases may permit automated detection and expansion of such a database to other regions susceptible to hail, such as Canada, Argentina, and Australia. Our expectation is that creation of this database will further the understanding of severe weather damage by hail and wind to agriculture and help address prediction and mapping of damage outcomes.

Acknowledgments. The authors would like to acknowledge the NASA Applied Sciences Disasters Program for providing resources in support of this research. The authors also acknowledge their colleagues on the Disasters Team at Marshall Space Flight Center who served as a soundboard and provided feedback during the development of this database and manuscript. Finally, the authors would like to acknowledge the three reviewers who took time to provide insightful comments and feedback to enhance the quality of this manuscript.

Data availability statement. The Hail and Wind Damage Swath Event Database will be available for public use after the successful publication of this manuscript (https://github.com/jrbell1/hwds_db). The public release of the database is being prepared with help from NASA's Interagency Implementation and Advanced Concepts Team (IMPACT; https://impact.earthdata.nasa.gov/) which has previously assisted in releasing datasets for public use including formatting open-source metadata and data preparation.

APPENDIX

Physical Characteristics Summary

In Table A1, we display a summary of length and width statistics measured using the manual and MBR methodologies and area summary.

TABLE A1. Summary table of length and width statistics measured using the manual and MBR methodologies and area summary.

	Maximum		Average		Minimum	
	Manual	MBR	Manual	MBR	Manual	MBR
			Length (km)			
All	372.5	377.3	29.0	28.7	2.1	2.1
Circular	14.0	14.7	6.0	6.0	2.1	2.1
Complex	184.0	185.5	43.4	42.3	11.2	11.4
Curved	253.4	237.3	31.3	30.2	3.6	3.6
Linear	372.5	377.3	29.1	28.9	2.9	2.9
			Width (km)			
All	29.5	37.0	6.1	6.8	1.4	1.5
Circular	14.2	11.5	5.6	5.3	2.1	1.7
Complex	29.5	32.8	12.6	13.9	3.2	5.5
Curved	23.9	37.0	6.4	8.1	1.7	1.9
Linear	24.9	33.0	5.8	6.3	1.4	1.5
			Area (km^2)			
All	4996.3		160.6		3.2	
Circular	130.1		30.5		3.2	
Complex	3291.7		381.5		35.5	
Curved	1660.1		162.9		6.3	
Linear	4996.3		157.6		3.7	

REFERENCES

American Farm Bureau Federation, 2023: New estimates reveal major 2022 weather disasters caused over $21 billion in crop losses date. Accessed 15 March 2023, https://www.fb.org/market-intel/new-estimates-reveal-major-2022-weather-disasters-caused-over-21-billion-in-crop-losses.

Bang, S. D., and D. J. Cecil, 2019: Constructing a multifrequency passive microwave hail retrieval and climatology in the GPM domain. *J. Appl. Meteor. Climatol.*, **58**, 1889–1904, https://doi.org/10.1175/JAMC-D-19-0042.1.

Bell, J. R., and A. L. Molthan, 2016: Evaluation of approaches to identifying hail damage to crop vegetation using satellite imagery. *J. Oper. Meteor.*, **4**, 142–159, https://doi.org/10.15191/nwajom.2016.0411.

——, E. Gebremichael, A. L. Molthan, L. A. Schultz, F. J. Meyer, C. R. Hain, S. Shrestha, and K. C. Payne, 2020: Complementing optical remote sensing with synthetic aperture radar observations of hail damage swaths to agricultural crops in the central United States. *J. Appl. Meteor. Climatol.*, **59**, 665–685, https://doi.org/10.1175/JAMC-D-19-0124.1.

Bentley, M. L., T. L. Mote, and P. Thebpanya, 2002: Using Landsat to identify thunderstorm damage in agricultural regions. *Bull. Amer. Meteor. Soc.*, **83**, 363–376, https://doi.org/10.1175/1520-0477-83.3.363.

Cecil, D. J., and C. B. Blankenship, 2012: Toward a global climatology of severe hailstorms as estimated by satellite passive microwave imagers. *J. Climate*, **25**, 687–703, https://doi.org/10.1175/JCLI-D-11-00130.1.

Changnon, S. A., Jr., 1967: Areal-temporal variations of hail intensity in Illinois. *J. Appl. Meteor.*, **6**, 536–541, https://doi.org/10.1175/1520-0450(1967)006<0536:ATVOHI>2.0.CO;2.

——, 1971: Hailfall characteristics related to crop damage. *J. Appl. Meteor.*, **10**, 270–274, https://doi.org/10.1175/1520-0450(1971)010<0270:HCRTCD>2.0.CO;2.

——, 1972: Examples of economic losses, from hail in the United States. *J. Appl. Meteor.*, **11**, 1128–1137, https://doi.org/10.1175/1520-0450(1972)011<1128:EOELFH>2.0.CO;2.

——, 1977: The scales of hail. *J. Appl. Meteor.*, **16**, 626–648, https://doi.org/10.1175/1520-0450(1977)016<0626:TSOH>2.0.CO;2.

——, and G. E. Stout, 1967: Crop-hail intensities in central and northwest United States. *J. Appl. Meteor.*, **6**, 542–548, https://doi.org/10.1175/1520-0450(1967)006<0542:CHIICA>2.0.CO;2.

Cintineo, J. L., T. M. Smith, V. Lakshmanan, H. E. Brooks, and K. L. Ortega, 2012: An objective high-resolution hail climatology of the contiguous United States. *Wea. Forecasting*, **27**, 1235–1248, https://doi.org/10.1175/WAF-D-11-00151.1.

Frisby, E. M., 1962: Relationship of ground hail damage patterns to features of the synoptic map in the upper Great Plains of the United States. *J. Appl. Meteor.*, **1**, 348–352, https://doi.org/10.1175/1520-0450(1962)001<0348:ROGHDP>2.0.CO;2.

——, 1963: Hailstorms of the upper Great Plains of the United States. *J. Appl. Meteor.*, **2**, 759–766, https://doi.org/10.1175/1520-0450(1963)002<0759:HOTUGP>2.0.CO;2.

Gallo, K., T. Smith, K. Jungbluth, and P. Schumacher, 2012: Hail swaths observed from satellite data and their relation to radar and surface-based observations: A case study from Iowa in 2009. *Wea. Forecasting*, **27**, 796–802, https://doi.org/10.1175/WAF-D-11-00118.1.

——, P. Schumacher, J. Boustead, and A. Ferguson, 2019: Validation of satellite observations of storm damage to cropland with digital photographs. *Wea. Forecasting*, **34**, 435–446, https://doi.org/10.1175/WAF-D-18-0059.1.

Gunturi, P., and M. K. Tippett, 2017: Managing severe thunderstorm risk: Impact of ENSO on U.S. tornado and hail frequencies. WillisRe Tech. Rep., 5 pp., http://www.columbia.edu/~mkt14/files/WillisRe_Impact_of_ENSO_on_US_Tornado_and_Hail_frequencies_Final.pdf.

Hansen, M. C., R. S. Defries, J. R. G. Townshend, and R. Sohlberg, 2000: Global land cover classification at 1 km spatial resolution using a classification tree approach. *Int. J. Remote Sens.*, **21**, 1331–1364, https://doi.org/10.1080/014311600210209.

Kelly, D. L., J. T. Schaefer, and C. A. Doswell III, 1985: Climatology of nontornadic severe thunderstorm events in the United States. *Mon. Wea. Rev.*, **113**, 1997–2014, https://doi.org/10.1175/1520-0493(1985)113<1997:CONSTE>2.0.CO;2.

Klimowski, B. A., M. R. Hjelmfelt, M. J. Bunkers, D. Sedlacek, and L. R. Johnson, 1998: Hailstorm damage observed from the *GOES-8* satellite: The 5–6 July 1996 Butte–Meade storm. *Mon. Wea. Rev.*, **126**, 831–834, https://doi.org/10.1175/1520-0493(1998)126<0831:HDOFTG>2.0.CO;2.

Loomis, I., 2018: Hail causes the most storm damage costs across North America. *Eos*, **99**, https://doi.org/10.1029/2018EO104487.

MODAPS Services, 2022: MODIS/Terra data outages. NASA/GSFC, accessed 20 October 2022, https://modaps.modaps.eosdis.nasa.gov/services/production/outages_terra.html.

Molthan, A. L., J. E. Burks, K. M. McGrath, and F. J. LaFontaine, 2013: Multi-sensor examination of hail damage swaths for near real-time applications and assessment. *J. Oper. Meteor.*, **1**, 144–156, https://doi.org/10.15191/nwajom.2013.0113.

Murillo, E. M., and C. R. Homeyer, 2019: Severe hail fall and hailstorm detection using remote sensing observations. *J. Appl. Meteor. Climatol.*, **58**, 947–970, https://doi.org/10.1175/JAMC-D-18-0247.1.

——, ——, and J. T. Allen, 2021: A 23-year severe hail climatology using GridRad MESH observations. *Mon. Wea. Rev.*, **149**, 945–958, https://doi.org/10.1175/MWR-D-20-0178.1.

Ortega, K. L., T. M. Smith, K. L. Manross, K. A. Scharfenberg, A. Witt, A. G. Kolodziej, and J. J. Gourley, 2009: The Severe Hazards Analysis and Verification Experiment. *Bull. Amer. Meteor. Soc.*, **90**, 1519–1530, https://doi.org/10.1175/2009BAMS2815.1.

——, T. Sandmael, B. R. Smith, and A. E. Reinhart, 2023: Big radar-based data sets for severe weather research produced at CIWRO/NSSL: Recent, current, future work and collaboration opportunities. *22nd Conf. on Artificial Intelligence for Environmental Science*, Denver, CO, Amer. Meteor. Soc., 4A.3, https://ams.confex.com/ams/103ANNUAL/meetingapp.cgi/Paper/421343.

Parker, M. D., I. C. Ratcliffe, and G. M. Henebry, 2005: The July 2003 Dakota hailswaths: Creation, characteristics, and possible impacts. *Mon. Wea. Rev.*, **133**, 1241–1260, https://doi.org/10.1175/MWR2914.1.

Rouse, J. W., Jr., R. H. Haas, J. A. Schell, and D. W. Deering, 1974: Monitoring vegetation systems in the Great Plains with ERTS. *Third ERTS Symp.*, College Station, TX, Remote Sensing Center, Texas A&M University, 309–317, https://ntrs.nasa.gov/api/citations/19740022614/downloads/19740022614.pdf.

Smith, T. M., and Coauthors, 2016: Multi-Radar Multi-Sensor (MRMS) severe weather and aviation products: Initial operating capabilities. *Bull. Amer. Meteor. Soc.*, **97**, 1617–1630, https://doi.org/10.1175/BAMS-D-14-00173.1.

Tang, B. H., V. A. Gensini, and C. R. Homeyer, 2019: Trends in United States large hail environments and observations. *npj Climate Atmos. Sci.*, **2**, 45, https://doi.org/10.1038/s41612-019-0103-7.

Taszarek, M., J. T. Allen, P. Groenemeijer, R. Edwards, H. E. Brooks, V. Chmielewski, and S.-E. Enno, 2020: Severe convective storms across Europe and the United States. Part I: Climatology of lightning, large hail, severe wind, and tornadoes. *J. Climate*, **33**, 10 239–10 261, https://doi.org/10.1175/JCLI-D-20-0345.1.

Towery, N. G., 1980: Some applications of remote sensing of crop-hail damage in the insurance industry. ISWS/CIRC-143/80, Illinois Institute of Natural Resources, 18 pp., https://www.isws.illinois.edu/pubdoc/C/ISWSC-143.pdf.

——, G. M. Morgan Jr., and S. A. Changnon Jr., 1976: Examples of the wind factor in crop-hail damage. *J. Appl. Meteor.*, **15**, 1116–1120, https://doi.org/10.1175/1520-0450(1976)015<1116:EOTWFI>2.0.CO;2.

Tucker, C. J., 1979: Red and photographic infrared linear combinations for monitoring vegetation. *Remote Sens. Environ.*, **8**, 127–150, https://doi.org/10.1016/0034-4257(79)90013-0.

Williams, S. S., K. L. Ortega, T. M. Smith, and A. E. Reinhart, 2022: Comprehensive radar data for the contiguous United States: Multi-year reanalysis of remotely sensed storms. *Bull. Amer. Meteor. Soc.*, **103**, E838–E854, https://doi.org/10.1175/BAMS-D-20-0316.1.

Witt, A., M. D. Eilts, G. J. Stumpf, E. D. W. Mitchell, J. T. Johnson, and K. W. Thomas, 1998: Evaluating the performance of WSR-88D severe storm detection algorithms. *Wea. Forecasting*, **13**, 513–518, https://doi.org/10.1175/1520-0434(1998)013<0513:ETPOWS>2.0.CO;2.